


Starch-based antibacterial food packaging with ZnO nanoparticle

Prakash Kumar¹ · Sanjeev Gautam¹  ·
Deepika Bansal¹ · Ravneet Kaur²

Revised: 20 June 2023 / Accepted: 31 August 2023 / Published online: 28 September 2023
© Association of Food Scientists & Technologists (India) 2023

Abstract Starch-based biofilms with embedded nanoparticles (NPs) are used to wrap food in biodegradable packaging system that has high antibacterial action against a variety of microorganisms. In this study, ZnO NPs were synthesised using both a green synthesis approach utilising *Azadirachta indica* (Neem) and a chemical synthesis approach using the sol–gel technique. The structural and morphological properties of all synthesized NPs were characterized through XRD, UV–VIS, UV-DRS, FTIR, and FESEM analysis. Further, these NPs were employed in the development of starch-based biodegradable films. A meticulous comparative analysis was performed to evaluate the functional properties of the nanocomposites, encompassing crucial parameters such as film thickness, moisture content, swelling index, opacity, solubility, water vapor permeability, and tensile strength. In comparison to films embedded with chemically synthesised NPs (F1), nanocomposite with green synthesised NPs (F2) showed 15.27% greater inhibition against *Escherichia coli* growth and 22.05% stronger inhibition against *Staphylococcus aureus* bacterial strains. Based on the biodegradability

analysis, the nanocomposite film-F2 showed a 53.33% faster degradation rate compared to the film-F1. The developed films were utilized to assess the quality of both wrapped and unwrapped grapes, leading to the generalization of the research for the development of starch-based antibacterial and environmentally friendly food packaging material.

Keywords Starch biofilms · ZnO nanoparticles · Green synthesis · ROS · *Azadirachta indica*

Introduction

During the past three decades, the development of new economies has resulted in a doubling of plastic consumption, which has led to a rise in the use of conventional packaging material across a variety of industries. Since 1950s, more than 8.3×10^3 million metric tonnes of plastic have been produced, and their utilization has multiplied exponentially. Food and beverage packaging accounts for approximately 16% of all plastic produced over the past seven decades (Yates et al. 2021). Plastics have revolutionized the food industry, despite the fact that they are not completely biodegradable. According to Shaikh et al. (2021), more than 95% of plastic produced by petroleum industries is derived from non-renewable sources and does not endure physical, chemical, or biological degradation. Yates et al. (2021) have reported that environmentalists have detected plastic residues in the macro, micro, and nano scales, leading to pollution of the surrounding environment. The accumulation of these residues in the food chain and the subsequent release of hazardous substances, such as bisphenol-A (BPA) and ester of phthalic acid, into packaged food and beverages, have raised major concerns (Pestana et al. 2021).

Prakash Kumar and Deepika Bansal worked equally in this research.

Supplementary Information The online version contains supplementary material available at <https://doi.org/10.1007/s13197-023-05834-9>.

✉ Sanjeev Gautam
sgautam@pu.ac.in

¹ Advanced Functional Materials Lab., Dr. S.S. Bhatnagar University Institute of Chemical Engineering and Technology, Panjab University, Chandigarh 160 014, India

² Department of Zoology, Panjab University, Chandigarh 160-014, India

Biopolymers, which are also referred to as biodegradable polymers, have become a feasible substitute for non-biodegradable plastics in various industrial sectors, especially in the food industry (Dey et al. 2021). These polymers are categorized as polymer derived from monomers, polymers generated from microorganisms, and polymers extracted from biomass, respectively (Shaikh et al. 2021). The market demand for biodegradable packaging materials is rising every day due to environmental and food safety concerns. In the food industry, researchers are concentrating on the development of biopolymers with enhanced biodegradable, antimicrobial properties, and functional properties comparable to synthetic polymers. Food packaging materials are more readily biodegradable when they contain polysaccharides such as cellulose, pullulan, agarose, starch, and chitosan. Moreover, the incorporation of metal nanoparticles (NPs) with some medicinal leaf extract into the polymeric network of biopolymer enhances their antimicrobial properties (Kumar et al. 2020a, b). The entire quality of the packaging material is influenced by the mechanical, physical, thermal, and barrier properties.

Biodegradable polymers derived from starch necessitate the inclusion of a plasticizer due to their high hydrophilicity, difficulty in refining, and brittleness (Mahuwala et al. 2020). Sorbitol, which is used in conjunction with starch films as a plasticizer, strengthens the films mechanical properties and impacts their ability to absorb moisture. Young modulus of synthesised biopolymer gets enhanced with addition of 40% (w/w) sorbitol with significant textural properties (Napierała and Stangierski 2007). Ghasemlou et al. (2011) developed edible kefir films using glycerol and sorbitol at the ratio of 10–25% (w/w) and found that the mechanical property and water vapor permeability (WVP) increases with increase in glycerol concentration. In addition, they concluded that at high plasticizer concentrations, phase separation led to an adhesive surface on glycerol-plasticized film and crystallization on sorbitol-plasticized films. Cao et al. (2007) examined gelatin films incorporated with ferulic acid and tannin acid and discovered that these two had cross-linking effects that provide mechanical strength at pH levels of 7 and 9, respectively. Wang et al. (2017) studied the mechanical and solubility properties of corn starch-collagen composite films and discovered that the thickness and opacity of the films increase with the addition of starch to collagen. As biopolymer have the potential for renewability, biodegradability, and replacement of toxic compounds, their development holds great promise for addressing a variety of sustainability issues (Ju et al. 2019). Therefore, the starch modification method is utilized to improve the functional properties of starch films, including films solubility, tensile strength, biodegradability, WVP, etc. (Slavutsky and Bertuzzi 2016).

Leng et al. (2022) stated that elevated respiration rate, ethylene synthesis, oxidative reactions, and enzymatic

browning are known to contribute to a reduction in the shelf life of perishable products. Their shelf life could be maintained by developing packaging material with great barrier and antimicrobial properties. Kumar et al. (2020a, b) analysed a variety of biodegradable nanocomposites for their antibacterial activity against gram positive and gram-negative bacteria for packaging bananas, papayas, guava, grapes, plums, tomatoes, and strawberries for an extended period of time. Indumathi et al. (2019) evaluated the shelf life of black grapes packaged in chitosan-cellulose acetate phthalate films containing ZnO NPs. They concluded that biopolymer increased the shelf life of grapes by up to 9 days, with the film biodegrading by 30–50% in 28 days. Ju et al. (2019) devised a composite film composed of khorasan wheat starch and moringa leaf extract with enhanced antioxidative and biodegradability property. Kumar et al. (2019) synthesised the green approach nanocomposite film using *Mimusops elengi* and demonstrated the efficacy of ZnO NPs in preventing the deterioration of green grapes for 14–21 days. Starch is inherently nontoxic, odorless, and colorless, and it has a high potential for film formation; therefore, its use in food packaging and coating is justified.

Several researchers have synthesised various types of inorganic metal oxide NPs like, ZnO, SiO₂, MgO₂, TiO₂, and CuO; ZnO is the most desirable because it is safe, inexpensive, and can be easily fabricated into nanowires, nanoflakes, a nanobelt, nanoflowers, and nanorods (Kumar et al. 2020a, b). The Food and Drug Administration has recognized ZnO as GRAS material with regulation number of 21CFR182.8991. Using a Trojan horse strategy and reactive oxygen mechanism, ZnO NPs can enhance the efficacy of biopolymer by inhibiting the proliferation of pathogenic microorganisms responsible for contamination (Zare et al. 2022). On the basis of the characteristics and potential use of ZnO NPs, it has been the subject of current research among other nanomaterials. The addition of 0.2% ZnO NPs improved the textural and antimicrobial properties of soy isolate protein films by 231% and 16%, respectively (Tang et al. 2019). Ma et al. (2016) synthesised ZnO NPs and applied a coating of these NPs to ordinary paper using a laboratory paper coater.

Green synthesis is considered a highly promising method for synthesising NPs owing to their biocompatibility, minimal toxicity, and environmentally sustainable properties. Vijayakumar et al. (2021) analysed the application of neem gum as a capping and stabilising agent for the synthesised NPs. Additionally, it has been observed that the rate of biological synthesis reaction is equivalent to that of chemical synthesis reaction. Din et al. (2022) reported that the moisture content and percentage solubility of starch nanocomposites decreased as the ZnO NPs content increased. According to Sirelkhatim et al. (2015), the antibacterial activity of NPs increases as their size decreases. Furthermore, ZnO

NPs produced by green techniques exhibit antibacterial activity even at very low concentrations of bacteria (Zare et al. 2022).

In the current study, nanocomposite biofilms were created using synthesised ZnO NPs, corn starch, plasticizer (glycerol), and crosslinking agent (acetic acid). The ZnO NPs were produced utilising a chemical synthesis approach (sol–gel technique) as well as a green (or biochemical) synthesis approach utilising *Azadirachta indica* (Neem). During the study, the influence of pH on crystallite size of ZnO NPs was also investigated. The literature on the development of starch-based biofilms using green synthesised ZnO NPs with neem extract is limited. It has been observed that there has not been much research on green grapes packaged in nanocomposite biofilms developed from neem extract. ZnO NPs embedded biofilms have tested against bacterial strains as it has immense potential to address food safety-related concerns.

Materials and methods

$\text{Zn}(\text{CH}_3\text{OO})_2 \cdot \text{H}_2\text{O}$, KOH, NaOH, and acetic acid were purchased from Sigma-Aldrich (India), whereas corn starch (CS) and glycerol were purchased from Loba Chemical Pvt. Ltd. (India). *Escherichia coli* (*E. coli*; gram negative) and *Staphylococcus aureus* (*S. aureus*; gram positive) bacterial strains were obtained from CSIR-IMTECH, Chandigarh, India. Neem leaves were collected from the botanical garden, Panjab University, Chandigarh (India).

Sol–gel approach for synthesis of ZnO NPs

ZnO NPs were synthesised by direct precipitation method, 1 M solution of $\text{Zn}(\text{CH}_3\text{OO})_2 \cdot \text{H}_2\text{O}$ (as a precursor) and 1 M solution of KOH was taken. To maintain the correct pH levels, a titration was carried out at various pH levels of 8, 9, 10, and 11. After obtaining the desired pH, the white sol consistency solution was constantly agitated for 12 h at 28 ± 2 °C. The resulting sol was thoroughly rinsed with 100% pure $\text{C}_2\text{H}_5\text{OH}$ and centrifuged at 5000 rpm for 3 min. After heating the resulting $\text{Zn}(\text{OH})_2$ in a hot air oven at 80 °C for 15 h, the water vapours were evaporated, and the dried sample was completely crumpled using a mortar and pestle. Finally, ZnO NPs were produced by annealing at 450 °C for 1 h in a muffle furnace for obtaining more uniform crystal size NPs. Furthermore, researchers found that the crystallinity of the NPs increased as grain size increased during annealing (Padmavathy and Vijayaraghavan 2008). Figure S1 in supplementary text depicts a flowchart for the sol–gel synthesis of ZnO NPs.

Green synthesis of ZnO NPs using *Azadirachta indica* (neem)

Fresh Neem leaves extract preparation

Fresh neem leaves were cleaned, cut into slices, and then pulverized. The 2% and 3% concentrated solutions were created by dissolving 2 g and 3 g of the prepared paste in 100 cc of DI H_2O , and the prepared solution were then heated for 10 min at 100 °C. The necessary neem extract was then obtained through filtration using 1 Whatman filter paper (Fig. S2a).

Preparation of ZnO NPs by biochemical synthesis approach

Using 50 cc of the 2% and 3% neem leaf extract concentrations, a 2 mM zinc acetate dihydrate solution was formulated. Drop by drop, 1 M KOH solution was added until the desired pH (i.e., pH 10 and 11) of the entire solution remained constant until white precipitate sol consistency appeared. The pH range was selected based on the sol–gel synthesis process, which resulted in the attainment of the minimum size of the NPs. After that, centrifugation was carried out at 5000 rpm for 3 min, followed by thorough washing with 100% pure $\text{C}_2\text{H}_5\text{OH}$. The obtained sol was heated overnight at 80 °C in hot air oven. Water vapours from Zinc hydroxide were dehydrated after heating, and then sample was finely crushed with a mortar pestle. Finally, biochemically synthesised ZnO NPs were obtained by annealing treatment at 450 °C for 1 h in a muffle furnace (Fig S2b in supplementary text).

Development of ZnO NPs embedded biofilms

The solution casting and evaporation process was the main technique used for the synthesis of biofilms containing ZnO NPs (Fig. S3 in supplementary text). The synthesis techniques for ZnO were analysed to determine the smallest nanocrystals, which were then utilised in the synthesis of biofilms. For this method, 100 cc of DI water and 3 g of CS was added and swirled constantly. After that, synthesised NPs (100 mg) were added to the solution along with 30% (w/w) of glycerol to the added CS weight. A few drops of an acetic acid solution (5%) were added to maintain the pH between 3 and 4. The mixture was then heated at 90 °C for 30 to 45 min until its gelatinous consistency. The gelatinized solution was promptly sonicated at 90 °C for 5 min, and the resulting solution was subsequently vacuum-degassed. Finally, degassed homogenous solutions were poured into Petri dishes, evenly distributed, and incubated overnight at 25 ± 1 °C. The developed films were preserved in a desiccator at 25 ± 1 °C with $75 \pm 5\%$ RH until further investigation.

Table T1 (supplementary text) displays the nomenclature of the films that were developed. Three distinct biofilms were produced and named F1, F2, and F3. The objective of producing F1 and F2 was to achieve efficient nanocomposite films by incorporating ZnO NPs synthesised through the two aforementioned approaches, which possess a high volume to surface ratio (means minimum crystallite size).

The functional analysis of developed biofilms

The thickness of the developed nanocomposites was measured using a digital micrometre (MITUTOYO 293-821-30, Japan), which had a 0.001 mm precision. Six different locations on each sample were utilised to quantify its thickness, and the average value was used for analysis. Measurements were made in triplicate for all the biofilms identified functional properties. The moisture content (MC) of biofilms was determined by comparing the weight loss of films before and after drying in a laboratory oven at 105 ± 1 °C until a constant weight was reached (Chiumarelli and Hubinger 2012). The MC of the biofilms was measured in triplicate. Using the method developed by Cao et al. (2007), the swelling index (SI) was calculated with some modifications. In this experiment, square specimens (side length: 20 mm) were cut from the synthesised biofilms, dried in a laboratory oven at 105 ± 1 °C for 24 h, and then weighed. The dried specimen was immersed in distilled water for 2 min and then removed. After that blotting paper was used to remove the surface water molecules from the swollen specimen before it was weighed again. The amount of adsorbed water (or SI) was calculated by using Eq. (1):

$$\text{Swelling index}(\%) = \frac{(w_a - w_b)}{w_a} \times 100 \tag{1}$$

where, w_a and w_b are the weight of wet and hot air-dried sample, respectively.

The opacity (OP) of synthesised biofilms was evaluated using Hunter Lab colorimeter (Color Flex EZ, USA) using Eq. (2).

$$\text{Opacity}(\%) = \frac{OP_w}{OP_b} \times 100 \tag{2}$$

where, OP_w is the opacity at white background and OP_b is the opacity at black background.

The Solubility (S) of the synthesised biofilms were measured using method developed by Echeverría et al. (2014). In this experiment, square specimens (side length: 20 mm) were cut from the synthesised films, dried in a hot air oven at 105 ± 1 °C for 24 h, and then weighed. The dried specimen was submerged into 50 ml distilled water at temperature of 22–25 °C for 24 h. Following the filtration (using Whatman 1 filter paper) of the samples, the non-solubilized material on

the paper was dried in a laboratory oven at 105 ± 1 °C for 24 h. This was performed with the intent of determining the percentage by weight of the water-insoluble fraction, as given in Eq. (3) below

$$S(\%) = \frac{(w_x - w_y)}{w_x} \times 100 \tag{3}$$

where, w_x and w_y are the weight of dried specimen and weight of insoluble part, respectively.

Using ASTM E 95–96, the WVP of synthesised biofilms was analysed. In this, the mouth of glass beaker containing anhydrous CaCl₂ was covered with synthesised biofilm (air tightly). The glass beaker was then placed in a desiccator containing pure distilled water. Then the whole setup of desiccator was then placed within an incubator with a temperature of 25 ± 1 °C. After a predetermined amount of time, the variation in weight of a modified glass beaker was determined. The sample’s WVP was determined using Eq. (4).

$$\text{WVP} = \frac{\frac{\Delta m}{t} \times x}{a(P_i - P_0)} \times 100 \tag{4}$$

where, $P_i - P_0$ is the pressure difference across the two sides of the biofilm and $\frac{\Delta m}{t}$, a , and x represents the weight gain rate, beaker area, and thickness of the wrapped biofilm, respectively.

Using ASTM D 882-91, the textual property of the synthesised biofilms were analysed using Texture Analyzer (TA. XT Plus, Stable Micro Systems (SMS), USA). Specimens were mounted between the analyser grips using clamps with an initial grip gap of 50 mm. It was run at a crosshead speed of 0.5 mm per minute until it broke. Using Eqs. (5) and (6), tensile strength (S) and elongation at break (e) were calculated, as below

$$\text{Tensile strength, TS(MPa)} = \frac{f_m}{a} \tag{5}$$

$$\text{Engations break, E}(\%) = \frac{(l_2 - l_1)}{l_1} \times 100 \tag{6}$$

where, f_m , a , l_1 , and l_2 are the maximum force, the sample area, initial and final distance between the grips, respectively.

With certain modifications, the soil buried test (Fig. S4 in supplementary text) was utilised to assess the biodegradability (BD) of the developed films (Table T1 in supplementary text). In this experiment, square specimens (side length: 10 mm) were cut from the synthesised films and then dried in an oven at 105 ± 1 °C for 24 h, and then weighed. Then, a mixture of uniformly sized soil and compost was placed inside plastic container and filling them to the top. The specimens were buried in that mixture 20 mm or below from the container mouths. A constant time interval of one week was

used to measure weight loss of films under controlled conditions inside desiccator (Babae et al. 2015). Equation (7) provides the biodegradability test for the produced biopolymer with or without ZnO NPs.

$$BD(\%) = \frac{(b_o - b_1)}{b_o} \times 100 \quad (7)$$

where, b_o and b_1 are the weight of the initial specimen sample and final weight of the sample after burial test, respectively.

Characterization of the synthesised NPs and developed nanocomposite biofilms

X-ray diffraction (XRD) of synthesised ZnO NPs and ZnO NPs embedded biofilms was carried out on a X'Pert PRO diffractometer (PANalytical, Netherlands) equipped with Cu $K\alpha$ radiation ($\lambda = 0.1541$ nm) at Bragg's angle ranging from 20° to 90° with 1° per min for better resolution. FESEM (FEI Quanta FEG 200 HRSEM) was used to study the morphology of the synthesised ZnO NPs. The interactions between the components of the biofilms were examined using FTIR spectroscopy (Shimadzu 8400, Japan) with a resolution of 4 cm^{-1} and a wavenumber range of $400\text{--}4000\text{ cm}^{-1}$. Microstructural analysis of developed films was measured using scanning electron microscopy (SEM) (JEOL JCM-6000 BENCHTOP, JEOL Ltd, Japan) and images were taken in the range of $300\text{--}2000\text{ cm}^{-1}$ magnification. Using a UV–visible spectrophotometer (Shimadzu, UV-2600) ZnO NPs were analysed in between the range of wavelength (λ) of $200\text{--}700$ nm. The transparency and ultraviolet light barrier properties of films were studied using UV–Visible (UV–Vis) diffuse reflectance spectroscopy (DRS) in the wavelength range of $250\text{--}800$ nm with a UV 2600 spectrophotometer (Shimadzu Co., Tokyo, Japan).

Antibacterial analysis

The conventional agar diffusion approach was used to test the nanocomposite solutions antibacterial affinity against *E. coli* and *S. aureus* bacterial strains in accordance with CLSI, M02-A12 recommendations with certain modifications. In this, Mueller–Hinton Broth (MHB) and Mueller–Hinton Agar (MHA) were prepared. Bacterial strains were grown for an entire night before being diluted in MHB to a cell density of 10^5 CFU/ml and then applied to MHA. In a sterile setting, plates were then allowed to dry for some time. Then, a 6 mm diameter well spaded on an MHA plate was treated with a nanocomposite solution (100 mg/ml). The plate was incubated for 24 h at 37°C . Based on the zone of inhibition around the rifampicin-infused well, antibacterial activity was measured. An active nanocomposite solution

and HPLC-grade sterile water were used as negative and positive controls, respectively. Nanocomposite films with improved morphology and functional characteristics were analysed for antibacterial properties.

Qualitative analysis

The consumer's acceptance of any product, particularly food products, is determined by its colour. The variation in surface colour of the sample was calculated in terms of L^* (lightness), a^* (red/green), and b^* (yellow/blue) using a calibrated Hunter Lab Colorimeter. Utilizing a white calibration plate ($L^* = 97.75$, $a^* = -0.49$, and $b^* = 1.96$), the equipment was calibrated prior to each measurement.

Each grape's weight was recorded independently in two batches during the duration of storage. For determining the weight loss (WL) of the grape, the following Eq. (8) is employed.

$$\text{Weight loss, WL (\%)} = \frac{(m_i - m_f)}{m_i} \times 100 \quad (8)$$

where, m_i and m_f are the average initial and final weights of the grapes during storage period of 7 days.

For measuring the total soluble solids (TSS), a sharp knife was used to separate the pulp from the grapes, which was then mashed in a mortar and pestle. The crushed pulp was then squeezed with a muslin towel and were measured using a refractometer with a range of 0–32%.

Grape juice (6 g) was diluted in 25 cc of DI H_2O before being poured to the conical flask and then 0.01 N NaOH was added to titrate it using phenolphthalein (1%) as an indicator. The acidity of the grape pulp was measured using citric acid at a ratio of 1 g per 100 g. The pH of grapes was tested while they were being stored using a pH meter (Syntronics system-362, Ahmadabad, India).

Finally, the samples visual aspect, colour, texture, flavour, and general acceptability of wrapped grapes (WG) and non-wrapped grapes (NWG) with developed biofilms were evaluated on 9-point hedonic scale. A panel of five semi-trained individuals conduct the sensory evaluation of WG and NWG samples in order to assess the quality and acceptability of the fruits.

Results and discussion

Structural analysis

Figure 1a represents the X-ray diffraction (XRD) patterns of annealed ZnO NPs synthesised via the sol–gel method, within the pH range of 8–11. The wurtzite structure of the ZnO NPs was confirmed using patterns analogous to the

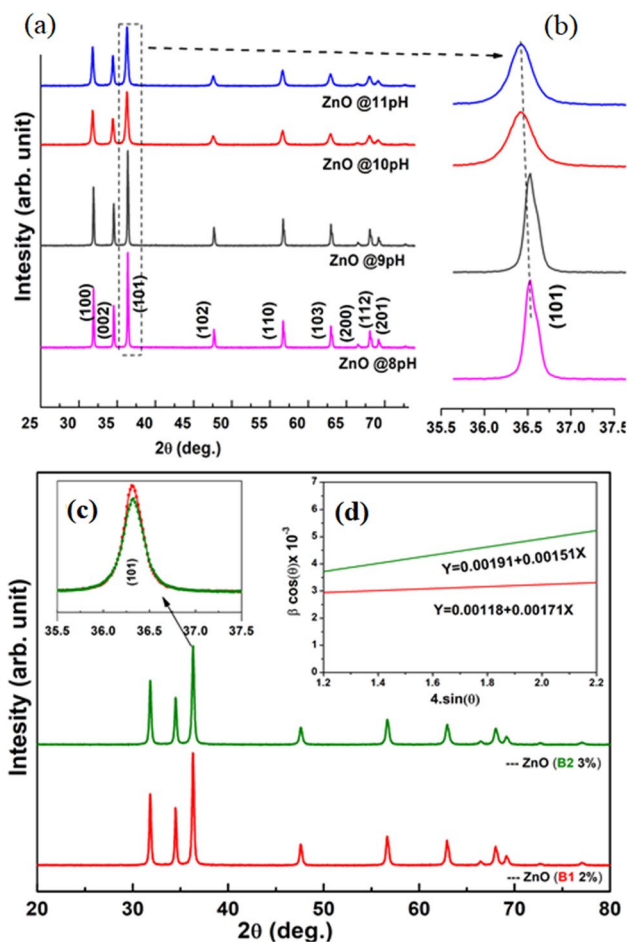


Fig. 1 a XRD patterns for sol-gel synthesised ZnO NPs at varied pH range of 8–11 with **b** broadening and lateral shift of significant peaks at $2\theta = 36.39^\circ$ (101) and XRD pattern for green synthesized ZnO NPs at varied neem concentration of 2% and 3%, indicated by B1 and B2, respectively. Here, in the XRD plot c indicates the broadening of the prominent peak at 2θ of 36.39° (101), and **d** indicates Williamson–Hall plot of NPs at 2% and 3% neem extract

XRD pattern documented on card number [01-070-2551] in the JCPDS database. The particles demonstrated a hexagonal crystal lattice and possessed a spherical morphology, which is also reported by Vijayakumar et al. (2021). Xu and Wang (2011) also discussed the relationship between the size of the crystallite and the pH of the solution. The dimensions of the ZnO nanocrystals were determined through the utilisation of the Debye–Scherer formula. Figure 1b shows the broadening and lateral shift of significant peaks at $2\theta = 36.39$ with varied pH levels. The impact of lattice strain on the properties of nanoparticles is noteworthy. The structural morphology of the ZnO NPs produced at pH 8 showed non-uniformity, with some impurities appearing as extra peaks. The Williamson–Hall (W–H) model was employed for the purpose of determining the average lattice strain present in ZnO NPs, as shown in Eq. (9).

$$\beta \cos \theta = \frac{K \lambda}{D_{hkl}} + 4 \epsilon \sin \theta \tag{9}$$

where, D_{hkl} is the NPs crystallite size, K is the structural constant (which is 0.89 for spherical ZnO NPs), λ is the X-ray wavelength (Cu $K\alpha$ radiation of 1.5418 \AA), β is the full width half maxima (FWHM), ϵ is the crystallite strain, and θ is the diffraction angle or Bragg’s angle.

The size of the crystallites decreases significantly, as the pH rises from 8 to 10, due to increase in lattice strain and stress in ZnO NPs. However, when the pH is further adjusted from 10 to 11, the crystallite size also increases due to the elevated alkalinity of the solution. The synthesis of ZnO NPs is typically impeded in the lower pH range, as a result of the elevated concentration of H^+ ions and reduced concentration of OH^- ions in the sol solution. Xu and Wang (2011) stated that pH impact on the formation of gel with subsequent hydrolysis and condensation behaviour of the solution has a significant influence on the morphology of ZnO. At pH 8, the largest crystallite observed i.e., 55.84 nm, while at pH 10, the smallest crystallite was observed i.e., 28 nm (Table T2 in supplementary text). Alias et al. (2010) synthesised the ZnO NPs with similar range of average particle size between 36.65 and 49.98 nm at varying pH range of 9–11. They stated that the particles size generally decreases when the pH of the sol increases above 9. Wu et al. (2019) relate the ZnO NPs length distribution and stated that most of the NPs have diameter in between 20 and 60 nm. Debye Scherrer’s formula was used to calculate the average crystalline size of ZnO NPs, as shown in following Eq. (10):

$$D_{hkl} = K \lambda / \beta \cos \theta \tag{10}$$

where, D_{hkl} , K , λ , β , and θ explained in Eq. (9).

During green synthesis of ZnO NPs, all XRD peaks correspond to JCPDS Card No. [01-070-2551], sharp peaks obtained in the XRD pattern revealed great crystallinity of synthesised NPs (Fig. 1c). At 2% and 3% of neem (*Azadirachta indica*) extract concentration, the crystallite size of ZnO were found to be 32.68 nm and 36.34 nm, respectively (Table T2 in supplementary text). The biochemical synthesised ZnO NPs was confirmed through UV–Vis spectroscopy. The lattice strain and lattice stress were responsible for the broadening of the prominent peak (Fig. 1d). The lattice strain inside the particle was also utilized to calculate the particle size using the W–H equation. As shown in Fig. 1 and Table T2 (supplementary text), as the lattice strain increases, the prominent peak expands, resulting in a slight reduction in the size of the ZnO NPs.

According to Sirelkhatim et al. (2015), the antibacterial activity of NPs increases as their size decreases. In order to create nanocomposite biofilms, Ma et al. (2016) synthesised ZnO NPs in the size range of 40–60 nm. They next studied the antibacterial and UV blocking properties of the NPs with

its sized reduction. They concluded that with reduced size of NPs led to a notable improvement in the bacterial inhibition against *E. coli*, which can be attributed to an increase in the surface-to-volume ratio (Padmavathy and Vijayaraghavan 2008). Therefore, considering these qualities, the smallest examined nanocrystals were then utilised for the further characterization and development of biofilms.

Ultraviolet-diffusive reflection spectroscopy (UV-DRS) and Ultraviolet-visible spectroscopy (UV-Vis) of the synthesised ZnO NPs

UV-DRS analysis revealed excellent optical properties with high band gap energies (E_g) of 3.11–3.19 eV (before annealing) and 3.12–3.25 eV (after annealing), as shown in Fig. S5 (supplementary text). It was discovered that the E_g of NPs varied with pH and annealing temperature. The study conducted by Sathianathan et al. (2023) revealed that the incorporation of ZnO nanoparticles into biopolymers resulted in the inhibition of harmful UV radiation, thereby preventing the instigation of oxidation in packaged food and ultimately enhancing the shelf life. According to López et al. (2021), exposure to UV radiation induces cleavage of the primary chain bond in the polymeric network of biofilm, which can be prevented by the incorporation of metal NPs with a high-energy gap. An elevated energy gap has been observed to enhance the overall structural stability of biopolymers.

Neem extract functions as a natural stabilising and reducing agent in green synthesis approach, which reduces the $\text{Zn}(\text{CH}_3\text{OO})_2 \cdot \text{H}_2\text{O}$ to ZnO. According to Ma et al. (2016) pure ZnO NPs show an absorbance peak at 380 nm under UV-Vis spectroscopy. Similar outcomes were found in the current study, where the UV absorbance peak for 2% and 3% neem extracts was found at 380 and 380.12 nm, respectively (Fig. S6 in supplementary text). The absorbance peaks were found to have changed due to variations in neem extract content.

FTIR spectroscopy analysis

The band at 3328.75–3336.10 cm^{-1} in ZnO NPs produced by sol-gel synthesis was assigned to the O–H vibration group. As the pH of the solution rises from 8 to 11, it was observed that the O–H peaks get narrow. Functional groups of C–O, C=O, and C–O–C, respectively, generated the strong asymmetric stretching in the regions 1647.97–1654.51 cm^{-1} , 1379.83–1379.97 cm^{-1} , and 1086.90–1086.97 cm^{-1} (Fig. S7a and Table T3 in supplementary text). Additionally, Alias et al. (2010) noted that in various alkaline conditions, these functional peaks alter as a result of divergence structural morphologies. On the other hand, green synthesised ZnO NPs showed the vibrational, stretching, and bending functional groups like O–H,

C–H, C–O, C=O, and C–O–C which were observed in the range of 3442.83–3450.21 cm^{-1} , 2927.51–2920.94 cm^{-1} , 1629.35–1635.92 cm^{-1} , 1382.36–1388.92 cm^{-1} , 1022.13–1028.69 cm^{-1} , respectively. The IR peaks ranged between 429.53 and 625.09 cm^{-1} (for chemically synthesised ZnO NPs) and 528.14–556.04 cm^{-1} (for green synthesised ZnO NPs) was due to the stretching of ZnO brought on by the conversion of $\text{Zn}(\text{OH})_2$ to ZnO (Fig. S7b and Table T4). Din et al. (2022) also observed the ZnO peaks in the range between 600 and 400 cm^{-1} . Alias et al. (2010) studied the ZnO peaks in 550–453 cm^{-1} range and observed some lateral shifts in the IR peaks, due to size difference in NPs on varying pH and plant extract concentration (Verma and Mehata 2016).

FE-SEM analysis of the synthesised ZnO NPs

As shown in Fig. 2, FESEM was used to analyse the morphology which includes the particle size and shape of the synthesised ZnO NPs. We may conclude from FESEM morphology that hexagonal and spherical ZnO nanostructures might be produced without the need of any catalytic material. It was believed that crystal growth and NPs nucleation were the two steps involved in the synthesis of ZnO NPs. In order to observe the differences in the alteration, the FESEM of two extreme crystallite sizes was investigated.

The size of NPs crystallites has been shown to change when the pH value increases from 8 to 11 (Table T2 in supplementary text). Divalent metal ions are believed to form in alkaline bases because they are unable to hydrolyse in acidic conditions. When ZnO NPs were generated at pH 10, their spherical and hexagonal structures revealed overall particle homogeneity. The overall chemical composition of produced NPs was determined using EDX Spectroscopy. Through EDX, it was possible to see that at pH 8, a mixture of three elements i.e., Zn, O, and C with atomic percentages of 47.48, 34.85, and 17.67, respectively, was existing (Fig. 2a). However, at pH 10 (Fig. 2b), we only discovered a mixture of two elements (i.e., Zn and O) with a larger atomic percentage. In synthesised ZnO NPs, the atomic ratio of Zinc to O was 1.36:1 at pH 8, but it was found to be 1.4:1 at pH 10, which is somewhat higher than the first one. Alias et al. (2010) reported similar results of morphological analyses for ZnO that were produced through the sol-gel technique, with pH values ranging from 6 to 11.

The utilisation of neem extract in the synthesis of ZnO NPs resulted in the production of more homogenous spherical-shaped nanostructures (Fig. 2c). The majority of the particles are spherical, and others are hexagonal in shape. Vijayakumar et al. (2021) have reported similar results in their morphological examination of ZnO nanoparticles that were produced using neem gum extract.

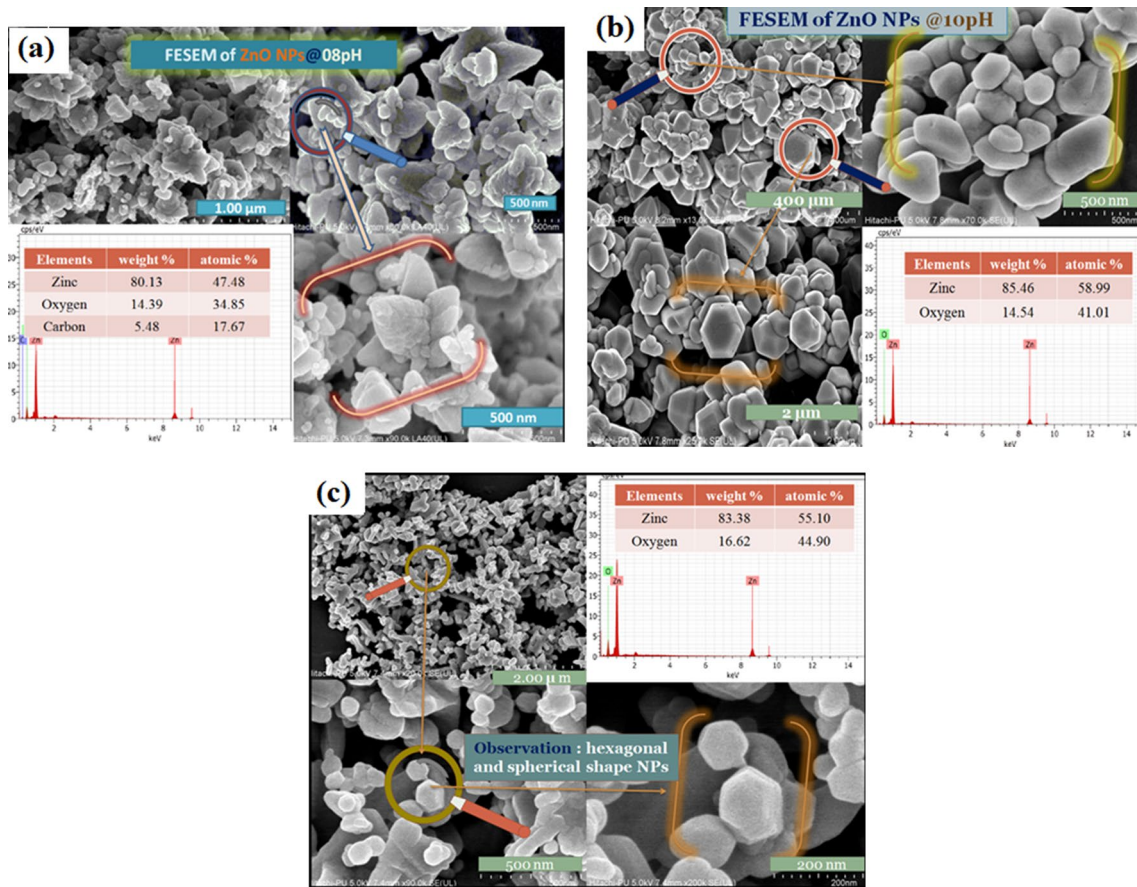


Fig. 2 FESEM micrographs of ZnO NPs synthesized using the sol–gel method at **a** pH of 8, **b** pH of 10, and **c** green synthesis of ZnO NPs using neem extract at pH of 10

Development and analysis of functional properties of ZnO NPs embedded biofilms

The current research analysed the functional characteristics of biofilms, namely F1 (Fig. S8), F2 (Fig. S9), and F3 (Fig. S10) which is shown in supplementary text. After being placed in a desiccator and exposed to a controlled atmosphere, the films were evaluated (Table 1 in supplementary text). Peighambardoust et al. (2019) stated that in order to improve the overall functional properties of biofilms, it is

essential to achieve a uniform distribution of the ZnO NPs in a biopolymeric network. According to Ghasemlou et al. (2011), the minimum concentration of glycerol required for effective results was 10% (w/w) based on the dry weight of the film. Films with glycerol concentrations below this level were observed to be fragile and challenging to handle, while those with glycerol concentrations exceeding 35% were noted to be flexible but adhesive. Hence, to ensure homogeneity and stability of the produced film, a fixed amount of 30 g of glycerol was utilised in the conducted experiment.

Table 1 Functional analysis of the developed biofilms (nomenclature of the films shown in Table T1)

Film	FT (mm)	MC (%)	SI (%)	OP (%)	S (%)	WVP × 10 ⁻¹¹ g (m s Pa) ⁻¹	TS (MPa)
F1	0.019 ± 0.003 ^a	09.98 ± 0.54 ^b	27.00 ± 0.35 ^c	29.19 ± 0.42 ^b	20.70 ± 0.74 ^b	2.42 ± 0.32 ^b	12.50 ± 0.18 ^a
F2	0.019 ± 0.009 ^a	10.13 ± 0.78 ^b	28.57 ± 0.14 ^b	30.43 ± 0.28 ^a	21.86 ± 0.42 ^b	2.85 ± 0.06 ^{ab}	12.36 ± 0.07 ^a
F3	0.014 ± 0.003 ^a	13.35 ± 0.25 ^a	45.24 ± 0.31 ^a	26.85 ± 0.28 ^c	27.55 ± 0.06 ^a	3.16 ± 0.14 ^a	9.12 ± 0.15 ^c

MC: Film thickness, MC: Moisture content, SI: Swelling index, OP: Opacity, S: Solubility, WVP: Water vapor permeability, TS: Tensile strength
 *Values having superscripts from a, b, and c differ significantly (p < 0.05) from each other column wise among different treatments based on Tukey’s test

The adhesive properties of films plasticized with glycerol may have arisen due to the occurrence of phase separation and glycerol diffusion towards the film surface. The functional properties of the developed biofilms are critically analysed as follows:

Film thickness (FT)

It was expected that the thickness of F1, F2, and F3 should change as NPs are added, but it was later found that this change in overall film thickness was non-significant ($p > 0.05$) (Table 1 in supplementary text). Similar trend in variation of thickness was obtained by Shankar et al. (2015) on addition of NPs into biopolymer. There exists a direct correlation between the thickness of films and the degree of molecular orientation and microstructure (Echeverría et al. 2014).

Moisture content (MC)

MC of the films decreased upon the addition of ZnO NPs. The biofilms embedded with ZnO NPs occupied the intermolecular space and form a hydrogen bonding in between the polymeric network which constrained the availability of the hydroxyl groups in the film matrix for further bonding, and this was also reported by Homthawornchoo et al. (2022). Therefore, Film F1 and F2 exhibited lower MC than F3, this is due to the fact that starch molecules have some affinity to absorb moisture. F1 and F2 exhibited a non-significant ($p > 0.05$) change in the MC of the film. Ghanbarzadeh et al. (2011) also reported that same hydrophilicity behaviour of starch molecule (Table 1 supplementary text).

Swelling index (SI)

Starch concentration and the SI of breaking of polymeric network of the films are said to be directly related. The H-bonding exists between the NPs and hydroxyl group in the polymeric matrix of the film decreases the hydrophilicity of the film. The SI of F2 was found to be significantly lower than that of F1 because neem served to cap the ZnO NPs that were located in between the polymeric network (Table 1 supplementary text). According to Ghanbarzadeh et al. (2011), the interaction of amylopectin and amylose with water changes significantly with the concentration of acetic acid and plasticizer. This was evident in F3, which simply comprised of acetic acid, plasticizer, and starch molecules.

Opacity (OP)

The addition of ZnO NPs to the starch polymeric network increased the OP of the embedded films. It was found that F2 exhibits the highest OP as compared to F1 and F3, this

could be possible due to the presence of neem constituents inside the film F2 (Table 1). According to Kim et al. (2017), citric acid caused cross-linking between the starch's crystalline and amorphous regions, resulting in reduced opacity. However, when the concentration of ZnO NPs incorporation was increased, it was possible that the nanocomposite film of starch-gelatin could experience some variation in opacity (Homthawornchoo et al. 2022).

Solubility (S)

In comparison to F1 and F2, film F3 exhibited the maximum solubility, because of the high hydrophilic nature of starch molecules (Table 1). Similar type of research was conducted by Homthawornchoo et al. (2022), where they synthesised the starch-gelatin nanocomposite films embedded with ZnO NPs. They observed that an increase in the concentration of NPs from 1 to 3% resulted in a decrease in the solubility of the film. This may be due to the ZnO NPs decreases the hydrophilicity of the starch polymeric network by occupying the intermolecular gaps and this was also reported by Lian et al. (2021). While film F1 and F2 have statistically non-significant S ($p > 0.05$), this could be possible due to ZnO NPs being capped by neem constituents, which reduces cohesiveness and thus stabilises the polymeric network. Verma and Mehata (2016) conducted a synthesis of Ag-NPs utilizing neem extract, and their study revealed that the presence of phytochemicals in neem played a crucial role in stabilizing the synthesized nanoparticles.

Water vapour permeability (WVP)

The water or moisture barrier properties of the packing material are related to water vapour permeability. Comparing the two films, F1 and F2, it was found that the WVP rate for both the films were significantly identical ($p < 0.05$), this could be possible due to the capping effect of neem constituents. F3 showed the significantly higher WVP rate of $3.16 \pm 0.14 \times 10^{-11} \text{ g m}^{-1} \text{ s}^{-1} \text{ Pa}^{-1}$ (Table 1). The study conducted by Homthawornchoo et al. (2022) showed the addition of ZnO NPs in the nanocomposite films led to a significant decrease in WVP. Tamimi et al. (2021) also reported the same trend in falling of WVP with addition in ZnO NPs in a synthesized tapioca starch nanocomposite with value range between $5.05 \times 10^{-10} \text{ g m}^{-1} \text{ s}^{-1} \text{ Pa}^{-1}$ to $2.77 \times 10^{-10} \text{ g m}^{-1} \text{ s}^{-1} \text{ Pa}^{-1}$. The observed phenomenon can be attributed to the convoluted trajectory of water molecules as they traverse the film, as well as the significant interstitial gaps resulting from the aggregation of nanoparticles within the film matrix. These factors collectively contribute to an augmented effective path for moisture diffusivity. A SEM micrograph of the films was used to further illustrate the mechanism of moisture migration in the films. Biofilms possess enhanced water vapour

and gas barrier properties, rendering them highly valuable and appealing for utilisation in food packaging applications.

Tensile strength (TS)

As shown in Table 1, it was found that TS readily increases with the addition of ZnO NPs. This may be due to the ZnO NPs occupying the intermolecular gaps which could increase the compactness of the film and this was also reported by Lian et al. (2021). When comparing films F1, F2, and F3, we found that F1 and F2 significantly showed the higher TS ($p > 0.05$), whereas F3 (10.22 ± 0.11 MPa) exhibited the lower TS, because of the increased hydrophilicity. Glycerol with NPs and cross-linking agents boosts the tensile strength of the synthesised films, which was also reported by Delavari and Stiharu (2022). Elongation (%) was found between 73.56% for F3, 103.67% for F2, and 105.32% for F1. Seligra et al. (2016) found that the starch film's elongation reduced and its TS increased with citric acid concentration. The types and concentrations of plasticizers have an impact on the physical and mechanical stability of the biodegradable films (Babae et al. 2015). The elastic limit is calculated using the modulus of elasticity, which measures the elastic behaviour of materials.

Biodegradability analysis of the synthesised biofilms

Table T5 (supplementary text) shows that F3 degraded quickly, followed by F1 and F2. Comparing F1 and F2; F2 degrades more quickly than F1 by 53.33%, this could be possible because of the capping effect of neem extract over the ZnO. The biofilms embedded with ZnO NPs occupied the intermolecular space and form a hydrogen bonding in between the polymeric network which constrained the availability of the hydroxyl groups in the film matrix for further bonding and thus improved the overall stability of the film with its compactness. Similar methodology was used by Babae et al. (2015) to explain a similar deterioration of nanocomposite starch films.

Characterization of synthesised nanocomposite biofilms

XRD analysis of the developed nanocomposite films

The XRD patterns of synthesised biofilms are shown in Fig. 3a. The sharp peaks in the XRD pattern that correspond to the significant peaks at $2\theta = 17.09^\circ$, 19.73° , and 22.11° of films F1 and F2 confirmed the presence of starch molecules with

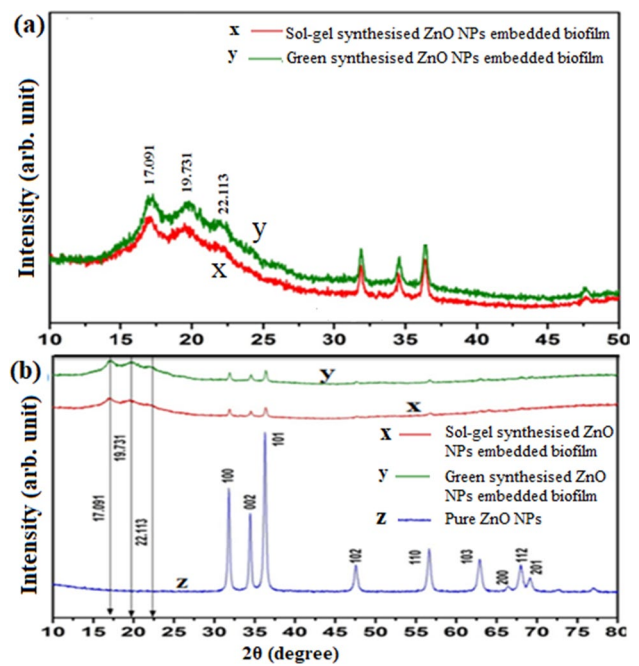


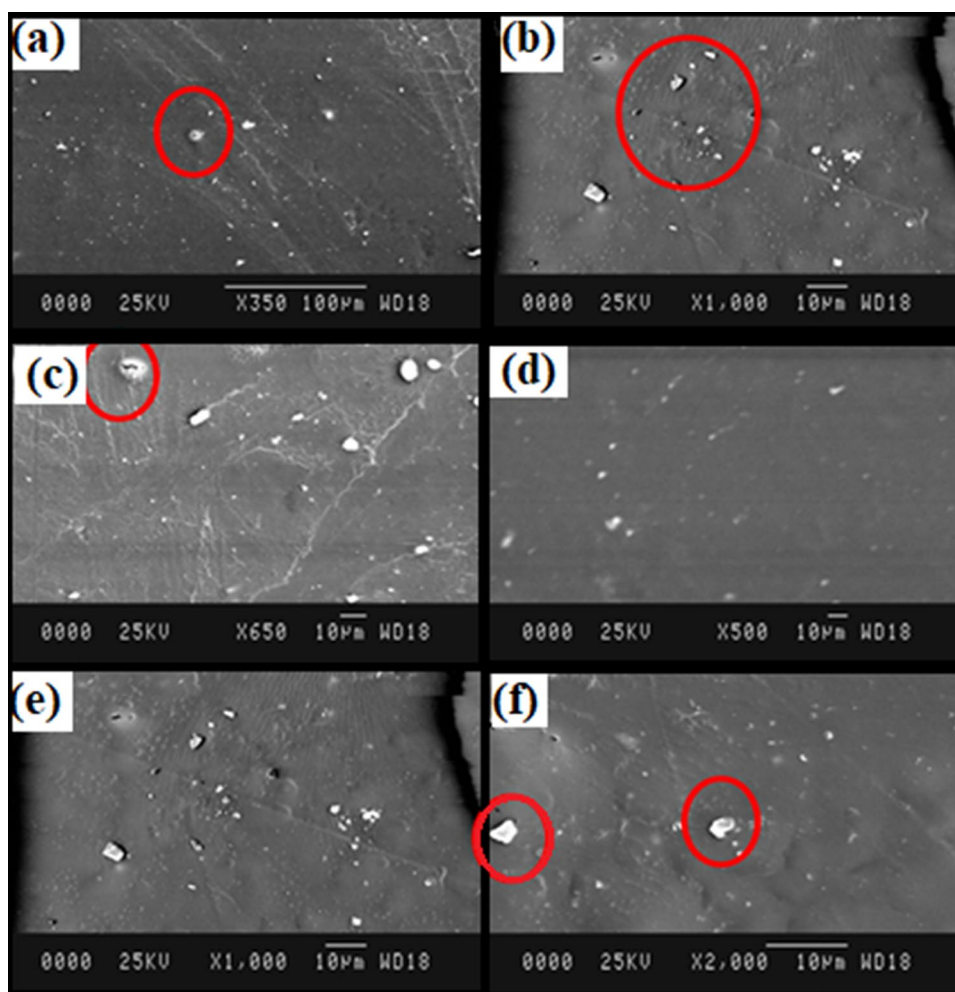
Fig. 3 XRD pattern of **a** biochemically synthesised ZnO NPs embedded film (y) and chemically synthesized ZnO NPs embedded film (x), and **b** comparison between XRD patterns of F1, F2, and pure ZnO NPs

low crystallinity, however on comparing with pure wurtzite structure of ZnO (Fig. 3b) confirmed the presence of ZnO NPs embedded in ZnO-starch nanocomposite, which is also reported by Ma et al. (2016). The prominent peak $2\theta = 36.28^\circ$ (101), indicating that ZnO NPs had no negative effect on the overall structural stability of the nanocomposite film, similar result is also shown by Lian et al. (2021). The analysis of Fig. 3 revealed broadening of the peaks, which may be attributed to the neem constituents capping and stabilising effect on the ZnO NPs which prevents the agglomeration by the action of steric hindrance within the polymeric network. The starch crystallinity increases when heated to a temperature of between 90 and 100 °C due to retrogradation and decreased with gelatinization (Kumar et al. 2020b).

Scanning electron microscopy (SEM) analysis of the developed nanocomposite films

ZnO NPs are evenly dispersed, as shown in the SEM images at various resolutions (Fig. 4). The synthesised nanocomposite films were primarily composed of glycerol and citric acid, which contributed to their uniformity and surface texture. The occurrence of surface roughness with some noticeable cracks in F1, indicated by the red circles, was presumed to be caused by the clustering of ZnO. This outcome was consistent with the findings of Hu et al. (2019) in their research

Fig. 4 SEM micrographs of (a–c) sol-gel synthesised ZnO NPs embedded biofilms (F1) at magnification of; (a) $\times 350$, (b) $\times 1000$, and (c) $\times 650$ at 100 μm , 10 μm , and 10 μm range, respectively, and (d–f) green synthesised ZnO NPs embedded biofilms (F2) at magnification of; (a) $\times 500$, (b) $\times 1000$, and (c) $\times 2000$ at 10 μm



on ZnO-chitosan nanocomposite films. It was observed that F2 (Fig. 4d–f) were smoother and more homogeneous than F1 (Fig. 4a–c), this could be possible due to the presence of neem constituents which stabilizes the NPs more uniformly between the intermolecular space of the polymeric network. This gives more compactness and uniform structure without any noticeable cracks or roughness.

Antibacterial analysis of the ZnO NPs embedded nanocomposite biofilms

Nanocomposites embedded with green synthesised NPs (F2) showed 15.27% greater inhibition against *E. coli* growth and 22.05% stronger inhibition against *S. aureus* bacterial strains compared to F1, a significant result has been shown in Table 2 and Fig. S11 (supplementary text). This could be because the synthesised green ZnO NPs have a capped neem constituents coating, which itself exhibits antibacterial characteristics. Verma and Mehata (2016) also examined the antibacterial activity of nanocomposite films with presence of neem extract. Additionally, the

Table 2 Zone of Inhibition of ZnO NPs embedded starch biofilm solution (nomenclature of the films shown in Table T1)

Bacterial strain	NPs embedded Film	Inhibition zone(mm)
<i>E. coli</i>	F1 solution	12 ± 0.24^b
	F2 solution	14 ± 0.11^a
<i>S. aureus</i>	F1 solution	5 ± 0.17^b
	F2 solution	6 ± 0.31^a

*Values having superscripts from a and b differ significantly ($p < 0.05$) from each other column wise among different treatments based on Tukey's test

results revealed that *S. aureus* displayed higher susceptibility compared to *E. coli* and similar results has been observed by Hu et al. (2019). The observed phenomenon can be attributed to the variations in the cellular wall composition between the two bacterial species. Many researchers reported the antibacterial properties of ZnO NPs against both gram-positive and gram-negative bacterial strains (Ma et al. 2016; Peighambardoust et al. 2019; Tamimi et al. 2021; Zare et al. 2022).

Qualitative analysis of wrapped grapes (WG) and non-wrapped grapes (NWG)

F2 was selected for the quality assessment of wrapped grapes because it more effectively inhibited bacterial strains with excellent functional characteristics and favourable biodegradability tests. In this experiment, one set of green grapes was wrapped in F2 (represented by wrapped grapes, or WG), and the other set was not, as represented by non-wrapped grapes, or NWG. The physiochemical properties of grapes i.e., pH, colour, total soluble solids (TSS), and acidity were observed for seven days at 28 ± 2 °C (Table T6 in supplementary text). Kumar et al. (2020b) evaluated the efficacy of biodegradable nanocomposites in preserving the quality and shelf life of packaged perishable fruits against chemical, enzymatic, and microbial degradation.

It was observed that the WG showed much better results than NWG. The WG maintains more moisture than NWG; during the course of 7 days of storage, there was a weight variation of almost 11.21% in WG, whereas 63.39% in NWG. The TSS of grapes typically rises with storage time, and in WG and NWG, the TSS probably increased by 7.72% and 18.48%, respectively. The acidity of the NWG decreases more readily than WG. Zheng et al. (2022) discovered a similar relationship between TSS and acidity for grapes stored at 25 °C and 4 °C. The pH of the WG and NWG was found to have decreased by 4.651% and 25.19%, respectively. The carbohydrates of grapes undergo conversion during storage, resulting in the production of organic acids that contribute to a decrease in pH (Leng et al. 2022). The overall colour (ΔE) change of WG and NWG was 3.49% and 12.07%, respectively. The overall acceptance for WG and NWG in the 9-point hedonic scale (Table T7 supplementary text) parameter was 7.8 and 4, respectively (Table T8 supplementary text). As a result, the biofilms with embedded ZnO-neem NPs prolong the shelf life of the wrapped grapes with retaining their excellent quality and widespread acceptance. Kumar et al. (2019) synthesised the nanocomposite film through green approach using *Mimusops elengi* and demonstrated the efficacy of ZnO NPs in preventing the deterioration of green grapes for 14–21 days. Similarly, Indumathi et al. (2019) evaluated the shelf life of black grapes packaged in chitosan-cellulose acetate phthalate films containing ZnO NPs.

The phytochemical constituents present in neem, such as polyphenols, flavonoids, and terpenoids, exhibit strong binding properties and can effectively coat the surface of ZnO NPs. Furthermore, neem's bioactive compounds contribute to the enhanced antimicrobial, antioxidant, and anti-inflammatory properties of the ZnO NPs (Verma and Mehata 2016; Mocanu et al. 2019). The Food and Drug Administration has recognized ZnO as GRAS material with regulation number of 21CFR182.8991 (Zare et al.

2022). Additionally, the utilization of phytochemical-capped ZnO NPs reduce the oxidative stress imposed by free radicals on erythrocytes, thereby augmenting their resistance against haemolysis (Zare et al. 2019; Homthawornchoo et al. 2022). Akbar et al. (2021) investigated the cytotoxic effects of ZnO NPs on human cell lines at a concentration of 3:1 (mg/ml). Their findings revealed minimal cytotoxicity associated with the tested ZnO NPs in the experimental conditions employed. However, it remains crucial to undertake thorough and extensive research, accompanied by meticulous studies, to evaluate both the scale and mechanisms underlying the migration of NPs from food packaging materials into food products.

Conclusion

Starch is inherently nontoxic, odorless, and colorless, and it has a high potential for film formation; therefore, its use in food packaging and coating is justified. The addition of ZnO NPs seems to improve the biofilms overall functional properties. At 2% and 3% *Azadirachta indica* (Neem) extract concentration, the synthesised crystallite size of ZnO NPs were found to be 32.68 and 36.34 nm, respectively. The characterisation of the synthesised ZnO NPs were analysed using XRD, UV-DRS, UV-VIS, FTIR, and FESEM. It was analysed that pH impact on the formation of gel with subsequent hydrolysis and condensation behaviour of the solution has a significant influence on the morphology of ZnO. The biofilm F2 was discovered to be smoother, more stable, and more efficient at inhibiting the growth of *Escherichia coli* and *Staphylococcus aureus* than the F1. During quality evaluation, WG maintained greater psychochemical properties such as weight, pH, colour, TSS, and acidity than NWG. The overall colour (ΔE) change of WG and NWG was 3.49% and 12.07%, respectively. The use of F2 prolongs the shelf life of packed grapes while maintaining both their quality and general acceptability during quality inspections. It can be inferred that the nanocomposite film synthesised through an environmentally friendly approach exhibits significant effectiveness of ZnO NPs in mitigating the degradation of green grapes.

Authors' contributions Credit author statement: SG conceptualized, investigated, formal analysis, and did funding acquisition, project administration and supervision, DB wrote the original draft, literature investigation, discussion and revision, PK also wrote the original draft, methodology, investigation, experiment and discussion, and RK supported and discussed the antibacterial experiments.

Funding The research is supported by TEQIP-III (MHRD, Govt. of India) grants for Dr. SSB UICET, Panjab University, Chandigarh, India.

Data availability The data will be available on request. A statement has also been added to the manuscript.

Code availability Not applicable.

Declarations

Conflict of interest The authors affirm that they are free of any known financial conflicts of interest or close personal ties that may have looked to have acted on the research presented in this study.

Ethics approval Not applicable, original research article.

Consent to participate Not applicable.

Consent for publication The research article contains original data.

References

- AKBAR N, ASLAM Z, SIDDIQUI R et al (2021) Zinc oxide nanoparticles conjugated with clinically-approved medicines as potential antibacterial molecules. *AMB Exp*. <https://doi.org/10.1186/s13568-021-01261-1>
- ALIAS SS, ISMAIL AB, MOHAMAD AA (2010) Effect of pH on ZnO nanoparticle properties synthesized by sol–gel centrifugation. *J Alloys Compd* 499:231–237. <https://doi.org/10.1016/j.jallcom.2010.03.174>
- BABAE M, JONOBI M, HAMZEH Y, ASHORI A (2015) Biodegradability and mechanical properties of reinforced starch nanocomposites using cellulose nanofibers. *Carbohydr Polym* 132:1–8. <https://doi.org/10.1016/j.carbpol.2015.06.043>
- CAO N, FU Y, HE J (2007) Mechanical properties of gelatin films cross-linked, respectively, by ferulic acid and tannin acid. *Food Hydrocoll* 21:575–584. <https://doi.org/10.1016/j.foodhyd.2006.07.001>
- CHIUMARELLI M, HUBINGER MD (2012) Stability, solubility, mechanical and barrier properties of cassava starch–Carnauba wax edible coatings to preserve fresh-cut apples. *Food Hydrocoll* 28:59–67. <https://doi.org/10.1016/j.foodhyd.2011.12.006>
- DELAVARI MM, STIHARU I (2022) Preparing and characterizing novel biodegradable starch/PVA-based films with nano-sized zinc-oxide particles for wound-dressing applications. *Appl Sci (Switzerland)*. <https://doi.org/10.3390/app12084001>
- DEY A, DHUMAL CV, SENGUPTA P et al (2021) Challenges and possible solutions to mitigate the problems of single-use plastics used for packaging food items: a review. *J Food Sci Technol* 58:3251–3269
- DIN MI, SIDDIQUE N, HUSSAIN Z, KHALID R (2022) Facile synthesis of biodegradable corn starch-based plastic composite film reinforced with zinc oxide nanoparticles for packaging applications. *Inorg Nano-Metal Chem*. <https://doi.org/10.1080/24701556.2022.2081190>
- ECHEVERRÍA I, EISENBERG P, MAURI AN (2014) Nanocomposites films based on soy proteins and montmorillonite processed by casting. *J Memb Sci* 449:15–26. <https://doi.org/10.1016/j.memsci.2013.08.006>
- GHANBARZADEH B, ALMASI H, ENTEZAMI AA (2011) Improving the barrier and mechanical properties of corn starch-based edible films: effect of citric acid and carboxymethyl cellulose. *Ind Crops Prod* 33:229–235. <https://doi.org/10.1016/j.indcrop.2010.10.016>
- GHASSEMLOU M, KHODAIYAN F, OROMIEHIE A (2011) Physical, mechanical, barrier, and thermal properties of polyol-plasticized biodegradable edible film made from Kefiran. *Carbohydr Polym* 84:477–483. <https://doi.org/10.1016/j.carbpol.2010.12.010>
- HOMTHAWORNCHOO W, KAEWPRACHU P, PINIJSUWAN S et al (2022) Enhancing the UV-light barrier, thermal stability, tensile strength, and antimicrobial properties of rice starch–gelatin composite films through the incorporation of zinc oxide nanoparticles. *Polymers (Basel)*. <https://doi.org/10.3390/polym14122505>
- HU X, JIA X, ZHI C et al (2019) Improving the properties of starch-based antimicrobial composite films using ZnO–chitosan nanoparticles. *Carbohydr Polym* 210:204–209. <https://doi.org/10.1016/j.carbpol.2019.01.043>
- INDUMATHI MP, SAROJINI KS, RAJARAJESWARI GR (2019) International Journal of Biological Macromolecules Antimicrobial and biodegradable chitosan/cellulose acetate phthalate/ZnO nano composite films with optimal oxygen permeability and hydrophobicity for extending the shelf life of black grape fruits. *Int J Biol Macromol* 132:1112–1120. <https://doi.org/10.1016/j.ijbiomac.2019.03.171>
- JU A, BAEK SK, KIM S, BIN SK (2019) Development of an antioxidative packaging film based on Khorasan wheat starch containing moringa leaf extract. *Food Sci Biotechnol* 28:1057–1063. <https://doi.org/10.1007/s10068-018-00546-9>
- KIM HY, JANE J, LAMSAL B (2017) Hydroxypropylation improves film properties of high amylose corn starch. *Ind Crops Prod* 95:175–183. <https://doi.org/10.1016/j.indcrop.2016.10.025>
- KUMAR P, MAHAJAN P, KAUR R, GAUTAM S (2020a) Nanotechnology and its challenges in the food sector: a review. *Mater Today Chem*. <https://doi.org/10.1016/j.mtchem.2020.100332>
- KUMAR S, BORO JC, RAY D et al (2019) Bionanocomposite films of agar incorporated with ZnO nanoparticles as an active packaging material for shelf life extension of green grape. *Heliyon* 5:e01867. <https://doi.org/10.1016/j.heliyon.2019.e01867>
- KUMAR S, MUKHERJEE A, DUTTA J (2020b) Chitosan based nanocomposite films and coatings: emerging antimicrobial food packaging alternatives. *Trends Food Sci Technol* 97:196–209. <https://doi.org/10.1016/j.tifs.2020.01.002>
- LENG F, WANG C, SUN L et al (2022) Effects of different treatments on physicochemical characteristics of ‘Kyoho’ grapes during storage at low temperature. *Horticulturae*. <https://doi.org/10.3390/horticulturae8020094>
- LIAN R, CAO J, JIANG X, ROGACHEV AV (2021) Physicochemical, antibacterial properties and cytocompatibility of starch/chitosan films incorporated with zinc oxide nanoparticles. *Mater Today Commun* 27:102265. <https://doi.org/10.1016/j.mtcomm.2021.102265>
- LÓPEZ C, MEDINA K, AMBROSIO RD et al (2021) PLLA and cassava thermoplastic starch blends: crystallinity, mechanical properties, and UV degradation have arisen a growing interest in this material for various. *J Polym Res*. <https://doi.org/10.1007/s10965-020-02368-y>
- MAHUWALA AA, HEMANT V, MEHARWADE SD et al (2020) Synthesis and characterisation of starch/agar nanocomposite films for food packaging application. In: *IET nanobiotechnology*. Institution of Engineering and Technology, pp 809–814
- MA J, ZHU W, TIAN Y, WANG Z (2016) Preparation of zinc oxide–starch nanocomposite and its application on coating. *Nanoscale Res Lett*. <https://doi.org/10.1186/s11671-016-1404-y>
- MOCANU A, ISOPENCU G, BUSUIOC C et al (2019) Bacterial cellulose films with ZnO nanoparticles and propolis extracts: synergistic antimicrobial effect. *Sci Rep*. <https://doi.org/10.1038/s41598-019-54118-w>
- NAPIERAŁA DM, STANGIERSKI J (2007) Tensile properties of wheat starch film with the addition of sorbitol and albumin. *Acta Agrophys* 9:123–133
- PADMAVATHY N, VIJAYARAGHAVAN R (2008) Enhanced bioactivity of ZnO nanoparticles—An antimicrobial study. *Sci Technol Adv Mater*. <https://doi.org/10.1088/1468-6996/9/3/035004>

- Peighambaroust SJ, Peighambaroust SH, MohammadzadehPournasir N, Pakdel P (2019) Properties of active starch-based films incorporating a combination of Ag ZnO and CuO nanoparticles for potential use in food packaging applications. *Food Packag Shelf Life*. <https://doi.org/10.1016/j.fpsl.2019.100420>
- Pestana CJ, Moura DS, Capelo-Neto J et al (2021) Potentially poisonous plastic particles: microplastics as a vector for cyanobacterial toxins microcystin-LR and microcystin-LF. *Environ Sci Technol* 55:15940–15949. <https://doi.org/10.1021/acs.est.1c05796>
- Sathianathan RV, Sundararajan A et al (2023) Intelligent food packaging and shelf-life improvement of chapattis using hybrid nanoparticle-based biopolymer electrospin coating. *ACS Food Sci*. <https://doi.org/10.1021/acsfoodscitech.3c00012>
- Seligra PG, Medina Jaramillo C, Famá L, Goyanes S (2016) Biodegradable and non-retrogradable eco-films based on starch-glycerol with citric acid as crosslinking agent. *Carbohydr Polym* 138:66–74. <https://doi.org/10.1016/j.carbpol.2015.11.041>
- Shaikh S, Yaqoob M, Aggarwal P (2021) An overview of biodegradable packaging in food industry. *Curr Res Food Sci* 4:503–520
- Shankar S, Teng X, Li G, Rhim J (2015) Food hydrocolloids preparation, characterization, and antimicrobial activity of gelatin/ZnO nanocomposite films. *Food Hydrocoll* 45:264–271. <https://doi.org/10.1016/j.foodhyd.2014.12.001>
- Sirelkhatim A, Mahmud S, Seeni A et al (2015) Review on zinc oxide nanoparticles: antibacterial activity and toxicity mechanism. *Nanomicro Lett* 7:219–242
- Slavutsky AM, Bertuzzi MA (2016) Improvement of water barrier properties of starch films by lipid nanolamination. *Food Packag Shelf Life* 7:41–46. <https://doi.org/10.1016/j.fpsl.2016.01.004>
- Tamimi N, MohammadiNafchi A, Hashemi-Moghaddam H, Baghaie H (2021) The effects of nano-zinc oxide morphology on functional and antibacterial properties of tapioca starch bionanocomposite. *Food Sci Nutr* 9:4497–4508. <https://doi.org/10.1002/fsn3.2426>
- Tang S, Wang Z, Li W et al (2019) Ecofriendly and biodegradable soybean protein isolate films incorporated with ZnO nanoparticles for food packaging. *ACS Appl Bio Mater* 2:2202–2207. <https://doi.org/10.1021/acsabm.9b00170>
- Verma A, Mehata MS (2016) Controllable synthesis of silver nanoparticles using Neem leaves and their antimicrobial activity. *J Radiat Res Appl Sci* 9:109–115. <https://doi.org/10.1016/j.jrras.2015.11.001>
- Vijayakumar S, Divya M, Vaseeharan B et al (2021) Biogenic preparation and characterization of ZnO nanoparticles from natural polysaccharide *Azadirachta indica* L. (neem gum) and its clinical implications. *J Clust Sci* 32:983–993. <https://doi.org/10.1007/s10876-020-01863-y>
- Wang K, Wang W, Ye R et al (2017) Mechanical properties and solubility in water of corn starch-collagen composite films: effect of starch type and concentrations. *Food Chem* 216:209–216. <https://doi.org/10.1016/j.foodchem.2016.08.048>
- Wu Y, Gu Y, Tong L et al (2019) Electrochemical synthesis of ZnO nanoparticles and preparation of pea starch/ZnO composite for active food packaging application. *Int J Electrochem Sci* 14:10745–10753. <https://doi.org/10.20964/2019.12.38>
- Xu S, Wang ZL (2011) One-dimensional ZnO nanostructures: solution growth and functional properties. *Nano Res* 4:1013–1098
- Yates J, Deeney M, Rolker HB et al (2021) A systematic scoping review of environmental, food security and health impacts of food system plastics. *Nat Food* 2:80–87. <https://doi.org/10.1038/s43016-021-00221-z>
- Zare M, Namratha K, Ilyas S et al (2022) Emerging trends for ZnO nanoparticles and their applications in food packaging. *ACS Food Sci Technol*
- Zare M, Namratha K, Thakur MS, Byrappa K (2019) Biocompatibility assessment and photocatalytic activity of bio-hydrothermal synthesis of ZnO nanoparticles by *Thymus vulgaris* leaf extract. *Mater Res Bull* 109:49–59. <https://doi.org/10.1016/j.materresbu.2018.09.025>
- Zheng R, Xiong X, Li X et al (2022) Changes in polyphenolic compounds of Hutai No. 8 grapes during low-temperature storage and their shelf-life prediction by identifying biomarkers. *J Agric Food Chem* 70:15818–15829. <https://doi.org/10.1021/acs.jafc.2c06573>

Publisher's Note Springer Nature remains neutral with regard to jurisdictional claims in published maps and institutional affiliations.

Springer Nature or its licensor (e.g. a society or other partner) holds exclusive rights to this article under a publishing agreement with the author(s) or other rightsholder(s); author self-archiving of the accepted manuscript version of this article is solely governed by the terms of such publishing agreement and applicable law.